

# Strange mode instabilities and mass-loss in evolved massive primordial stars

Abhay Pratap Yadav,<sup>★</sup> Stefan Henrique Kühnrich Biavatti and Wolfgang Glatzel

*Institut für Astrophysik (IAG), Georg-August-Universität Göttingen, Friedrich-Hund-Platz 1, D-37077 Göttingen, Germany*

Accepted XXX. Received YYY; in original form ZZZ

## ABSTRACT

A linear stability analysis of models for evolved primordial stars with masses between 150 and 250  $M_{\odot}$  is presented. Strange mode instabilities with growth rates in the dynamical range are identified for stellar models with effective temperatures below  $\log T_{\text{eff}} = 4.5$ . For selected models the final fate of the instabilities is determined by numerical simulation of their evolution into the non-linear regime. As a result, the instabilities lead to finite amplitude pulsations. Associated with them are acoustic energy fluxes capable of driving stellar winds with mass-loss rates in the range between  $7.7 \times 10^{-7}$  and  $3.5 \times 10^{-4} M_{\odot} \text{ yr}^{-1}$ .

**Key words:** stars: massive – stars: mass-loss – stars: oscillations – stars: Population III – stars: supergiants – stars: winds, outflows

## 1 INTRODUCTION

Primordial stars with initially vanishing metallicity are cosmologically relevant in many respects: Being the only source for the production of metals they are responsible for chemical evolution in the early universe (see [Nomoto et al. 2013](#)). Thus they have an important influence on the formation and evolution of cosmic structure. Having masses up to  $\sim 1000 M_{\odot}$  they typically end their life as pair instability supernovae enriching their environment with heavy elements or leaving behind intermediate mass black holes (see, e.g., [Bromm & Larson 2004](#); [Ohkubo et al. 2009](#)). Being smaller and hotter than their counterparts with finite metallicity they are the most promising source of the reionization of the universe (see, e.g., [Tumlinson & Shull 2000](#); [Barkana & Loeb 2001](#); [Loeb & Barkana 2001](#)). Indication for the existence of primordial (Pop III) stars has meanwhile been found from the observations of high redshift galaxies (see, e.g., [Fosbury et al. 2003](#); [Kashlinsky et al. 2005](#)). The study presented in this paper of the structure and evolution of primordial stars including consideration of their stability is therefore of utmost importance for cosmology. Should an instability prevail which leads to pulsationally driven mass loss, it would be relevant not only for the evolution of Pop III stars but also for the enrichment with metals of the environment.

Investigations of the formation process of primordial stars indicate that the absence of metals allows for the formation of massive fragments with masses in the range

between 100 and 1000  $M_{\odot}$  (see, e.g., [Abel et al. 2000](#); [Bromm et al. 1999, 2002](#)). Whether these massive primordial Pop III stars suffer from significant mass-loss during their evolution or the evolution proceeds at constant mass, is still a matter of debate. Due to the absence of metals, line driven winds can be excluded as a source of mass-loss. A stability analysis of Pop III stars with respect to the  $\varepsilon$  - mechanism revealed instabilities which are too weak to drive a significant mass-loss ([Baraffe et al. 2001](#)). Moreover, this  $\varepsilon$  - instability is restricted to the very vicinity of the zero age main sequence. On the other hand, massive Pop III stars are characterized by high luminosity to mass ratios ( $>10^3$  in solar units) which imply a high fraction of the radiation pressure in the envelopes of these stars. Both high L/M ratios and dominant radiation pressure favour the occurrence of strange mode instabilities (see, e.g., [Glatzel 1994](#)). Therefore strange mode instabilities are to be expected in massive primordial stars.

The objective of the present study is to identify strange mode instabilities in massive primordial stars by a linear stability analysis and subsequently to determine the final result by numerical simulation of their evolution into the non-linear regime. Evolution and stability with respect to the  $\varepsilon$  - mechanism close to the main sequence has been studied by [Baraffe et al. \(2001\)](#). In the present study we shall therefore ignore this phase and restrict our investigation to the post main sequence phase, where the evolution proceeds at almost constant mass and luminosity from high to low effective temperature. Moreover, since the  $\varepsilon$  - mechanism is disregarded and the strange mode instabilities of interest

<sup>★</sup> E-mail: yadav@astro.physik.uni-goettingen.de

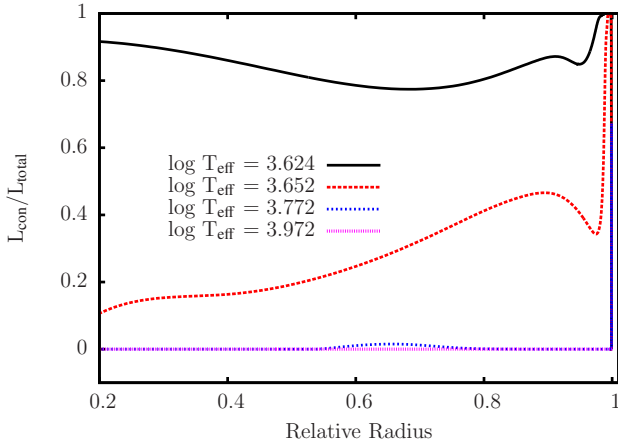


**Figure 1.** Ratio of convective and total luminosity as a function of relative radius for stellar models with  $M = 150 M_{\odot}$  and  $\log L/L_{\odot} = 6.6$  and the effective temperatures indicated. With decreasing effective temperature, the contribution of convection to the energy transport in the envelope increases significantly.

operate in the stellar envelope only, we can restrict ourselves to the consideration of envelopes.

The stellar models considered will be described in section 2, their linear stability analysis in sections 3 and 4. Non-linear simulation are discussed in section 5. A discussion and our conclusions follow (section 6).

## 2 MODELS

Concerning the objective to study strange mode instability of evolved massive primordial stars disregarding  $\varepsilon$  - instability, we restrict ourselves to the investigation of envelope models (rotation and magnetic fields are ignored) with masses of 150, 200 and 250  $M_{\odot}$ , respectively. In the post main sequence phase, evolution proceeds at almost constant mass and luminosity. Thus these masses correspond to a luminosity of  $\log L/L_{\odot} = 6.60, 6.77$  and  $6.88$ , respectively (see [Moriya & Langer 2015](#); [Baraffe et al. 2001](#)). The effective temperature is varied between  $\log T_{\text{eff}} = 4.80$  and  $\log T_{\text{eff}} = 3.62$ . For the chemical composition, we adopt primordial values  $Z = 0.00$ ,  $X = 0.77$  and  $Y = 0.23$ . Opacities are taken from the OPAL tables ([Rogers & Iglesias 1992](#); [Rogers et al. 1996](#); [Iglesias & Rogers 1996](#)).

For given mass, luminosity and effective temperature envelope models are constructed by integrating the equations of mass conservation, hydrostatic equilibrium and energy transport from the photosphere to a maximum cutoff temperature. To ensure that the parts of the envelope relevant for stability are represented, the latter has to be chosen sufficiently high. For the initial conditions of the integration, we have adopted Stefan-Boltzmann’s law and the common prescription for the photospheric pressure (see section 11.2 of [Kippenhahn et al. 2012](#)).

Concerning the energy transport, Schwarzschild’s criterion has been used for the onset of convection. Convection is treated according to the standard mixing length theory ([Böhm-Vitense 1958](#)) with 1.6 pressure scale heights for the mixing length. In models with effective temperatures above

$\log T_{\text{eff}} = 3.7$  energy transport by convection is negligible, below  $\log T_{\text{eff}} = 3.7$ , the fraction of convectively transported energy strongly increases with decreasing  $T_{\text{eff}}$ . This is illustrated in Fig. 1, where the ratio of the convective and the total luminosity is given as a function of relative radius for stellar models with different effective temperatures. Stellar models with  $\log T_{\text{eff}} \approx 3.6$  are fully convective.

## 3 LINEAR STABILITY ANALYSIS

The linear stability analysis is based on the equations governing linear stability and pulsations in the form given by [Gautschi & Glatzel \(1990b\)](#), equation 2.12). Together with four boundary conditions, they form a fourth order eigenvalue problem. It is solved using the Riccati method introduced by [Gautschi & Glatzel \(1990a\)](#). The eigenvalues are complex where the real parts ( $\sigma_r$ ) correspond to the pulsation frequency and the imaginary parts ( $\sigma_i$ ) provide information about excitation or damping of the corresponding mode. Negative values of the imaginary part ( $\sigma_i < 0$ ) indicate excitation and instability, positive values ( $\sigma_i > 0$ ) correspond to damping. In the following, eigenvalues will be normalized by the global free fall time  $\sqrt{\frac{R^3}{3GM}}$  ( $G$ ,  $R$  and  $M$  are the gravitational constant, radius and mass of the stellar model considered, respectively). For the normalization see also [Baker & Kippenhahn \(1962\)](#).

As a theory of the interaction of pulsation and convection is still not available, we have adopted for the treatment of convection the ‘frozen in approximation’ introduced by [Baker & Kippenhahn \(1965\)](#). In this approximation, the Lagrangian perturbation of the convective luminosity is disregarded in the pulsation equations. It is applicable as long as the convective turn over timescale is longer than the pulsation timescale and if the energy is mainly transported by radiation diffusion (see [Baker & Kippenhahn 1965](#), for a detailed discussion). For the models considered here, the frozen in approximation holds for  $\log T_{\text{eff}} > 3.7$ . However, as discussed in the previous section (see Fig. 1) below  $\log T_{\text{eff}} \approx 3.7$  convection is dominant and the results of the stability analysis have to be interpreted with caution.

## 4 RESULTS OF THE LINEAR STABILITY ANALYSIS

For the three masses 150, 200 and 250  $M_{\odot}$  and associated luminosities  $\log L/L_{\odot} = 6.60, 6.77$  and  $6.88$ , the results of the linear stability analysis, i.e., the real and imaginary parts ( $\sigma_r$ ,  $\sigma_i$ ) of the eigenvalues normalized by the global free fall time are presented as a function of the effective temperature in Figs. 2 - 7 which will be referred to as modal diagrams in the following. As long as the bottom boundary of the envelope is chosen sufficiently deep, the eigenfrequencies are neither sensitive to its position nor to the boundary conditions imposed there, which is a consequence of the common exponential decay of the eigenfunctions from the surface to the stellar core. For the boundary conditions at the photosphere, we have considered the conventional set, where the Lagrangian pressure perturbation is required to vanish and a linearized version of Stefan - Boltzmann’s law is assumed to hold (see [Baker & Kippenhahn](#)

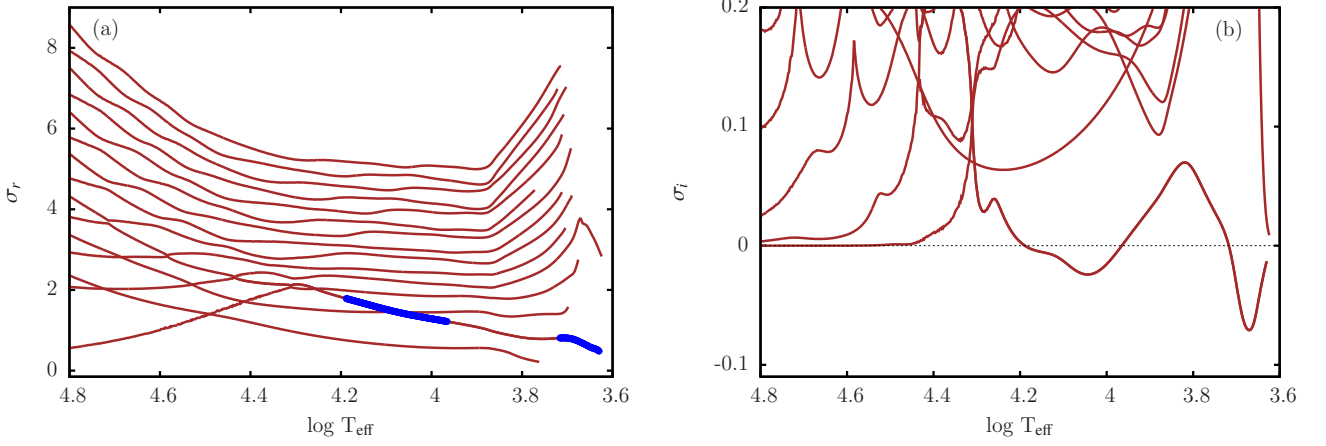


**Figure 2.** Real (a) and imaginary parts (b) of the eigenfrequencies normalized by the global free fall time as a function of effective temperature for stellar models with  $M = 150 M_{\odot}$  and  $\log L/L_{\odot} = 6.6$ . Unstable modes are indicated by thick lines in (a) and negative imaginary parts in (b). For the photospheric boundary conditions vanishing Lagrangian pressure perturbation and Stefan Boltzmann's law have been adopted.

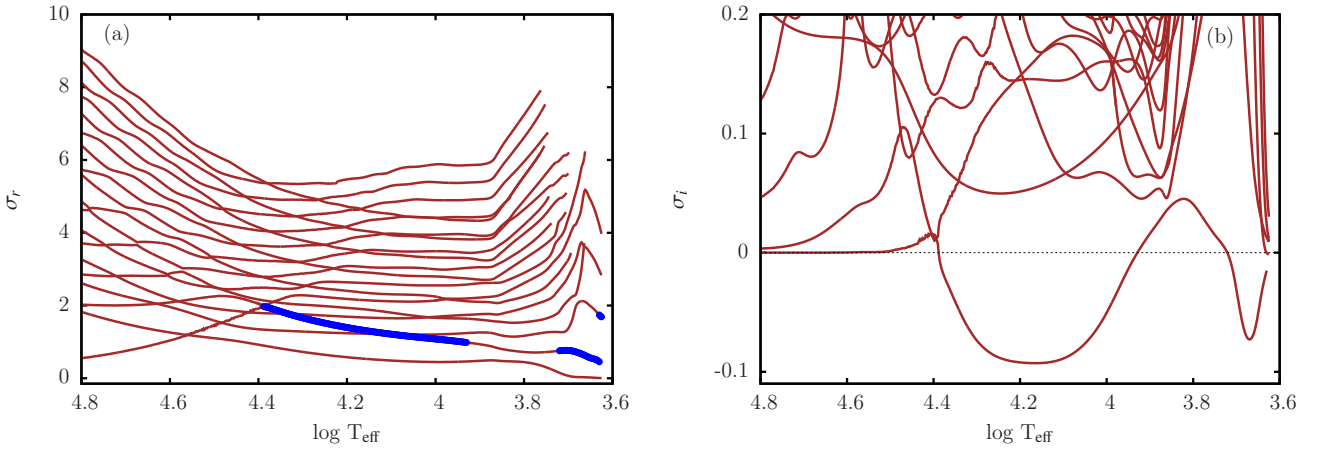


**Figure 3.** Same as Fig. 2 but for  $M = 200 M_{\odot}$  and  $\log L/L_{\odot} = 6.77$ .

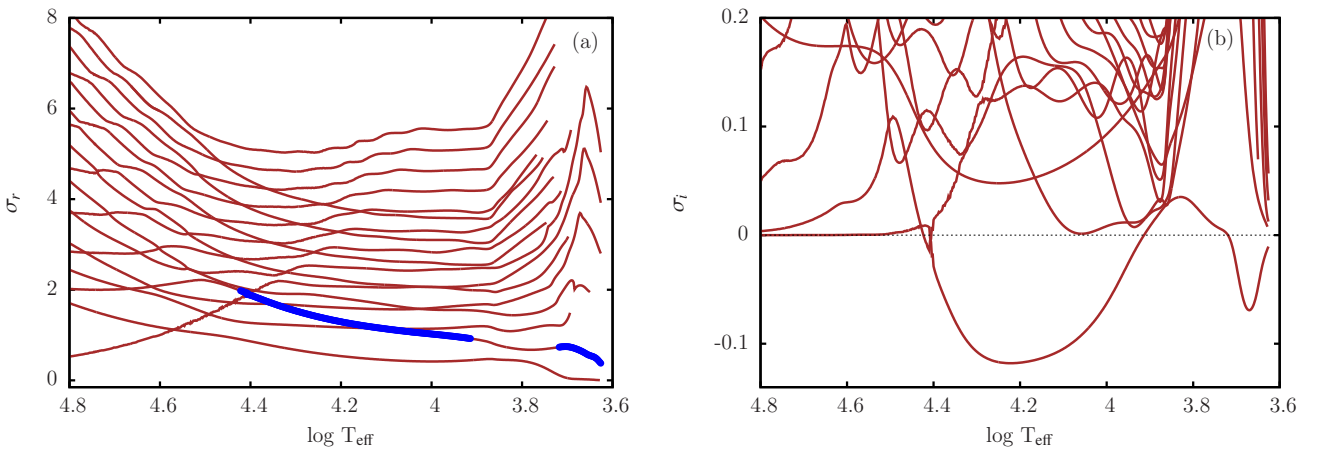


**Figure 4.** Same as Fig. 2 but for  $M = 250 M_{\odot}$  and  $\log L/L_{\odot} = 6.88$ .

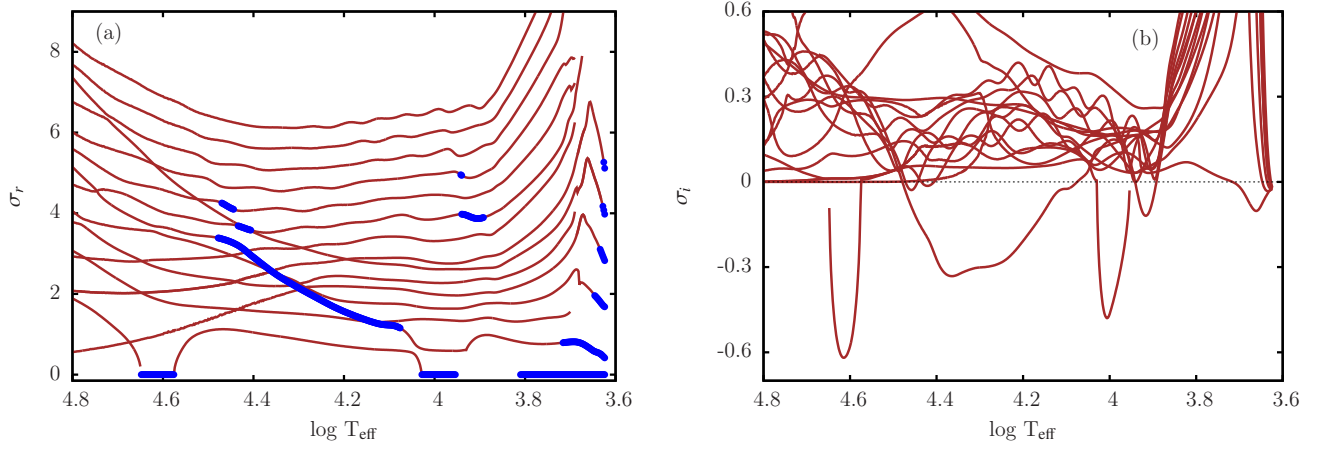


**Figure 5.** Same as Fig. 2 but for photospheric boundary conditions requiring the gradient of compression and the divergence of the heat flux to vanish.

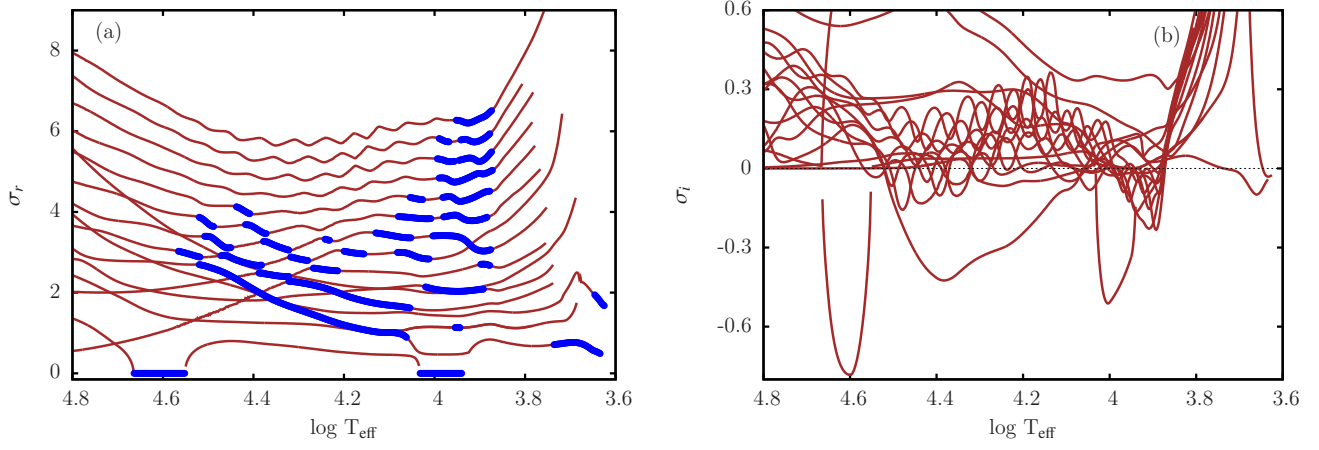


**Figure 6.** Same as Fig. 5 but for  $M = 200 M_{\odot}$  and  $\log L/L_{\odot} = 6.77$ .

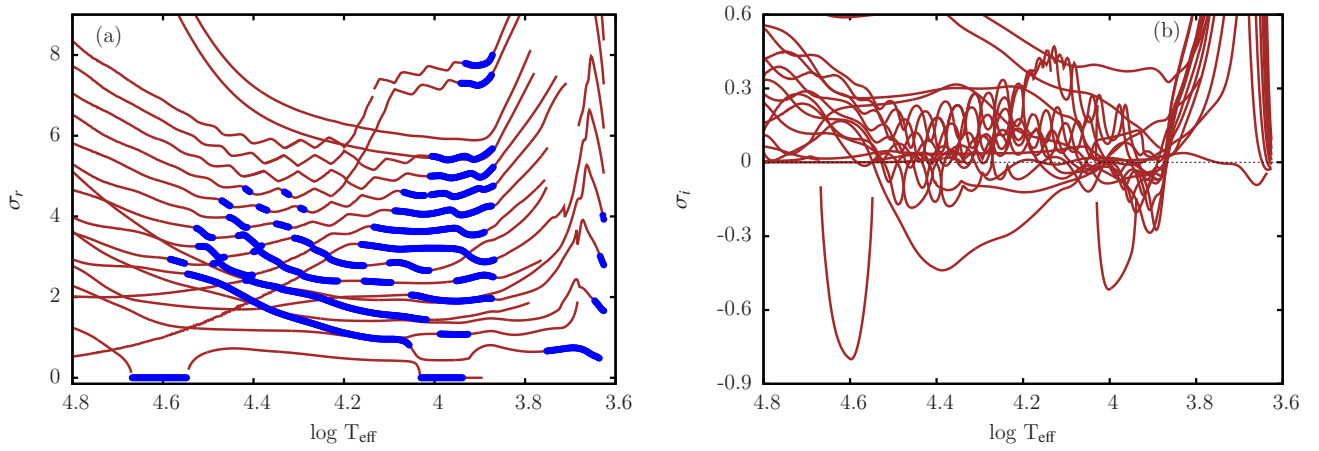


**Figure 7.** Same as Fig. 5 but for  $M = 250 M_{\odot}$  and  $\log L/L_{\odot} = 6.88$ .

1962). Alternatively, we have chosen boundary conditions which are identical with those used in the subsequent non-linear simulations. These boundary conditions requiring the gradient of compression and the divergence of the heat flux to vanish are constructed such that reflection of waves and shocks at the outer boundary is minimized (see [Grott et al. 2005](#)). For stellar models previously tested for linear stability, the choice of the photospheric boundary conditions was not crucial ([Yadav & Glatzel 2017a,b](#)). Even if occasionally quantitative differences were observed, the results of the linear stability analysis did qualitatively not depend on the outer boundary conditions. For the massive primordial models considered here we have performed a stability analysis both using the conventional outer boundary conditions (results are shown in the modal diagrams Figs. 2 - 4) and with the boundary conditions consistent with the subsequent non-linear treatment (results are shown in the modal diagrams Figs. 5 - 7).

The stability analysis of models with  $150 M_{\odot}$  using conventional boundary conditions (Fig. 2) exhibits a complex behaviour of the eigenvalues which is typical for the expected strange mode phenomenon (see, e.g., [Yadav & Glatzel 2016, 2017a,b](#)): At least two sets of modes can be identified by actual crossings and sequences of avoided crossings. One of the mode crossings has unfolded into an instability band implying instabilities with growth rates in the dynamical regime for effective temperatures between  $\log T_{\text{eff}} = 4.21$  and  $\log T_{\text{eff}} = 3.98$ . A second instability associated with the second lowest eigenfrequency  $\sigma_r$  is observed for effective temperatures below  $\log T_{\text{eff}} = 3.7$  (see Fig. 2). We emphasize that a classification in terms of fundamental modes and overtones is not applicable here due to significant deviations from adiabatic behaviour. In models with  $\log T_{\text{eff}} < 3.7$ , energy transport is dominated by convection. Thus the results of the stability analysis in this range, in particular the instability identified there, have to be interpreted with caution. Contrariwise, the strange mode instability for effective temperatures between  $\log T_{\text{eff}} = 4.21$  and  $\log T_{\text{eff}} = 3.98$  occurs in models where convective energy transport is negligible.

The stability analysis of models with  $200 M_{\odot}$  and  $250 M_{\odot}$  using conventional boundary conditions (Figs. 3 and 4) reveals results qualitatively similar to those for  $150 M_{\odot}$  (Fig. 2). With increasing mass (and luminosity) both the growth rate and the temperature range of the strange mode instabilities increases to  $4.4 > \log T_{\text{eff}} > 3.93$  ( $200 M_{\odot}$ ) and to  $4.42 > \log T_{\text{eff}} > 3.91$  ( $250 M_{\odot}$ ). On the other hand, both the growth rate and maximum effective temperature ( $\log T_{\text{eff}} = 3.7$ ) for the instability of the convectively dominated models is almost independent of mass (and luminosity).

Comparing the results of the stability analysis for boundary conditions consistent with the subsequent non-linear simulations (Figs. 5 - 7) with those based on the conventional outer boundary conditions (Figs. 2 - 4), we recover counterparts of the strange mode instability and the instability for  $\log T_{\text{eff}} < 3.7$ . The latter is not affected by the boundary conditions, whereas the strange mode instability has become stronger and affects more than a single mode. In addition, several dynamical monotonic instabilities are found. Obviously their existence is due to the special choice of boundary conditions. The outer boundary conditions are in principle ambiguous, since the outer boundary of the stellar model does not coincide with the boundary of the star.

Therefore the physical relevance of instabilities caused by special boundary conditions remains an open question. We shall discuss this issue again in connection with the simulations of the evolution of the instabilities into the non-linear regime and the final fate of unstable stellar models.

Contrary to our study, the stability analysis of massive primordial stars by [Moriya & Langer \(2015\)](#) has not revealed any instability for  $\log T_{\text{eff}} > 3.7$ , in particular not the strange mode instability extending up to  $\log T_{\text{eff}} \approx 4.5$ . Whether the code used by these authors is not capable to identify strange mode instabilities or an operating error has prevented the discovery of the instability needs further study. On the other hand, the instability for  $\log T_{\text{eff}} < 3.7$  identified by [Moriya & Langer \(2015\)](#) is confirmed. However, as already noted, this instability occurs in convectively dominated models, where the fundamental assumptions of the stability analysis are no longer valid. Thus the physical relevance of this instability is highly questionable and requires further investigations.

Our study might also be regarded as a test for the strange mode instability mechanism proposed by [Glatzel \(1994\)](#). In the limit of high luminosity to mass ratios and dominant radiation pressure, the dispersion relation for strange modes reduces to ([Glatzel 1994](#)):

$$\omega^2 = \pm i 2g\kappa_{\rho}k \quad (1)$$

where  $\omega$ ,  $k$ ,  $g$  and  $\kappa_{\rho}$  denote frequency, wave number, gravity and the logarithmic derivative of the opacity with respect to density, respectively. For finite  $k$  and  $g$ , this dispersion relation provides instability only if  $\kappa_{\rho}$  does not vanish. Thus apart from high  $L/M$  ratios and dominant radiation pressure,  $\kappa_{\rho} \neq 0$  is an additional requirement for the occurrence of strange mode instabilities. For massive primordial stars high  $L/M$  ratios and dominant radiation pressure prevail in all evolutionary phases. Close to the main sequence, the effective temperatures are sufficiently high, such that the matter in the envelope is completely ionized and the opacity is determined by electron scattering with  $\kappa_{\rho} = 0$ . As a consequence, strange mode instabilities should not occur. However, as soon as in the post main sequence phase the effective temperatures becomes sufficiently low for helium to recombine, bound-free transitions of helium determine the opacity implying  $\kappa_{\rho} \neq 0$ . Thus we expect strange mode instabilities to occur together with helium recombination below  $\log T_{\text{eff}} \approx 4.5$ . The findings of our study agree with these predictions.

## 5 NONLINEAR SIMULATIONS

For selected unstable models, the evolution of the instabilities has been followed by numerical simulation into the non-linear regime in order to determine their final fate. The numerical scheme used for this purpose is described in [Grott et al. \(2005\)](#). It is fully conservative with respect to energy, i.e., the energy balance is satisfied by the scheme intrinsically and locally. This property is essential for the simulation of stellar instabilities and pulsations, since the kinetic energy and the time integrated acoustic energy at the outer boundary are smaller than the dominant gravitational and internal energies (see equation 23 of [Grott et al. 2005](#)) by several orders of magnitude for stellar pulsations.



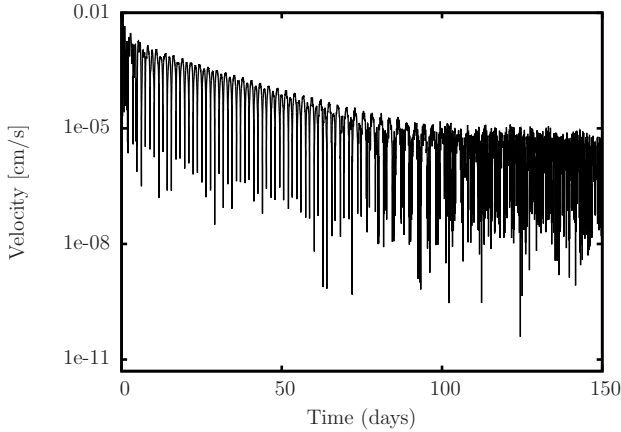


**Figure 8.** Velocity of the outermost grid point as a function of time for a model with  $M = 150 M_{\odot}$  and  $\log T_{\text{eff}} = 4.6$ . Consistent with the linear analysis the simulation exhibits a monotonic exponential increase saturating in the mildly non-linear regime. It is followed by an oscillatory exponential decay and ends on the numerical noise level. The final fate of this model is a new hydrostatic equilibrium with slightly different structure and parameters.

Thus for a meaningful determination of the kinetic energy and time integrated acoustic energy (at the outer boundary) which we are interested in, an extremely high accuracy is required which can only be achieved by using a fully conservative scheme. This issue has meanwhile been discussed and emphasized several times (see, e.g., [Grott et al. 2005](#); [Yadav & Glatzel 2016, 2017a,b](#)). As a consequence of conservativity, the numerical scheme has to be implicit with respect to time. In the course of the non-linear evolution of instabilities, shock waves do occur. They are represented by the introduction of artificial viscosity. For further details of the numerical treatment, we refer to [Grott et al. \(2005\)](#).

One term occurring in the energy balance of the system corresponds to the time integrated acoustic energy at the outer boundary (see equation 23 of [Grott et al. 2005](#)) representing the mechanical energy lost from the configuration by acoustic waves and shocks. As discussed in a previous paper ([Yadav & Glatzel 2017b](#)), there are phases of incoming and outgoing acoustic fluxes during a pulsation cycle. As a consequence, the time integrated acoustic energy is a non-monotonic function. However, integrated over one cycle the outgoing energy in general exceeds the incoming energy and on average the time integrated acoustic energy increases with time. Thus we obtain a mean slope of the integrated acoustic energy, which corresponds to a mean mechanical luminosity of the system (see [Yadav & Glatzel 2017b](#)). Assuming that this mean mechanical luminosity is responsible for mass-loss of the star, we can estimate the mass-loss rate by comparing it to the wind kinetic luminosity  $\frac{1}{2} \dot{M} v_{\infty}^2$ , where  $\dot{M}$  and  $v_{\infty}$  are the mass-loss rate and terminal wind velocity, respectively (see also [Grott et al. 2005](#); [Yadav & Glatzel 2016, 2017a,b](#)). The terminal wind velocity is estimated by the escape velocity. In this way, an estimate is obtained in the following for the mass-loss rate from the mean slope of the time integrated acoustic energy.

### 5.1 Models with masses of $150 M_{\odot}$

For models with masses of  $150 M_{\odot}$  ( $\log L/L_{\odot} = 6.6$ ) four unstable configurations with effective temperatures of  $\log T_{\text{eff}} = 4.6, 4.4, 4.2$  and  $4.0$  respectively have been selected for the numerical simulation of the evolution of the instabilities into the non-linear regime.

At  $\log T_{\text{eff}} = 4.6$ , a monotonic instability was identified using ‘minimum reflection boundary conditions’ (see Fig. 5), whereas this model turned out to be stable for the conventional boundary conditions (see Fig. 2). Starting from numerical noise, the evolution of the instability (see Fig. 8) exhibits a linear phase of monotonic exponential growth (with the growth rate predicted by the linear analysis) saturating at a weakly non-linear level (below  $0.01 \text{ cm/s}$  in terms of the velocity amplitude). At this phase a slight modification of the structure of the model implies stabilization. As a consequence, the model oscillates around its new equilibrium, i.e., we observe a damped oscillation ending - in terms of the velocity amplitude - on the numerical noise level superimposed on the new hydrostatic equilibrium.

At  $\log T_{\text{eff}} = 4.4$ , an oscillatory instability was identified using ‘minimum reflection boundary conditions’ (see Fig. 5), whereas this model turned out to be stable for the conventional boundary conditions (see Fig. 2). Starting from numerical noise, the evolution of the instability (see Fig. 9) exhibits a linear phase of (oscillatory) exponential growth (with period and growth rate as predicted by the linear theory) saturating after  $\approx 150$  days in the non-linear regime with a velocity amplitude of  $38 \text{ km s}^{-1}$ . After  $\approx 600$  days, the structure is sufficiently modified to ensure stabilization and the configuration starts to oscillate around a new hydrostatic equilibrium with an exponential decay of the superimposed perturbations. The decay of the velocity perturbations switches from oscillatory to monotonic around  $\approx 900$  days.

At  $\log T_{\text{eff}} = 4.2$ , an oscillatory instability was identified independent of the boundary conditions (see Figs. 5 and 2). After the linear phase of exponential growth non-linear saturation is reached for this model after  $\approx 600$  days with a velocity amplitude of  $\approx 30 \text{ km s}^{-1}$  (see Fig. 10b). Rather than a new hydrostatic equilibrium, finite amplitude pulsations are the consequence of the instability for this model. An increase of the mean radius by  $\approx 8$  per cent in the non-linear regime is found (see Fig. 10a) implying the final non-linear pulsation period of 13.3 days to be higher than predicted by the linear analysis. For illustration of the accuracy requirement and the numerical quality of the simulation, some terms occurring in the energy balance (see equation 23 of [Grott et al. 2005](#)) together with its error are displayed in Fig. 10(f)-(i). Potential and internal energy (Fig. 10h) have almost identical modulus and opposite sign. They exceed the kinetic (Fig. 10f) and the time integrated acoustic energy (Fig. 10g) by three and one order of magnitude, respectively, whereas the error in the energy balance (Fig. 10i) is smaller than the smallest term in the energy balance by at least two orders of magnitude. From the mean slope of the time integrated acoustic energy, we derive  $7.7 \times 10^{-7} M_{\odot} \text{ yr}^{-1}$  as an estimate for the mass-loss rate induced and driven by the pulsation.

Similar to the model with  $\log T_{\text{eff}} = 4.6$ , a monotonic instability was identified for  $\log T_{\text{eff}} = 4.0$  using ‘minimum reflection boundary conditions’ (see Fig. 5), whereas stability or very weak instability was found for the conven-

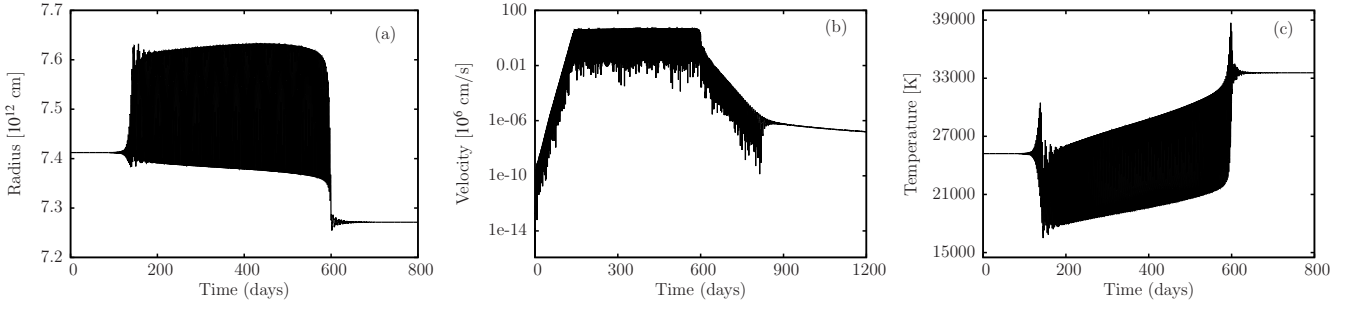


**Figure 9.** Evolution of instabilities into the non-linear regime for a model with  $M = 150 M_{\odot}$  and  $\log T_{\text{eff}} = 4.4$ . Radius (a), velocity (b) and temperature (c) at the outermost grid point are given as a function of time. The instability leads to a new hydrostatic state with modified structure and parameters.

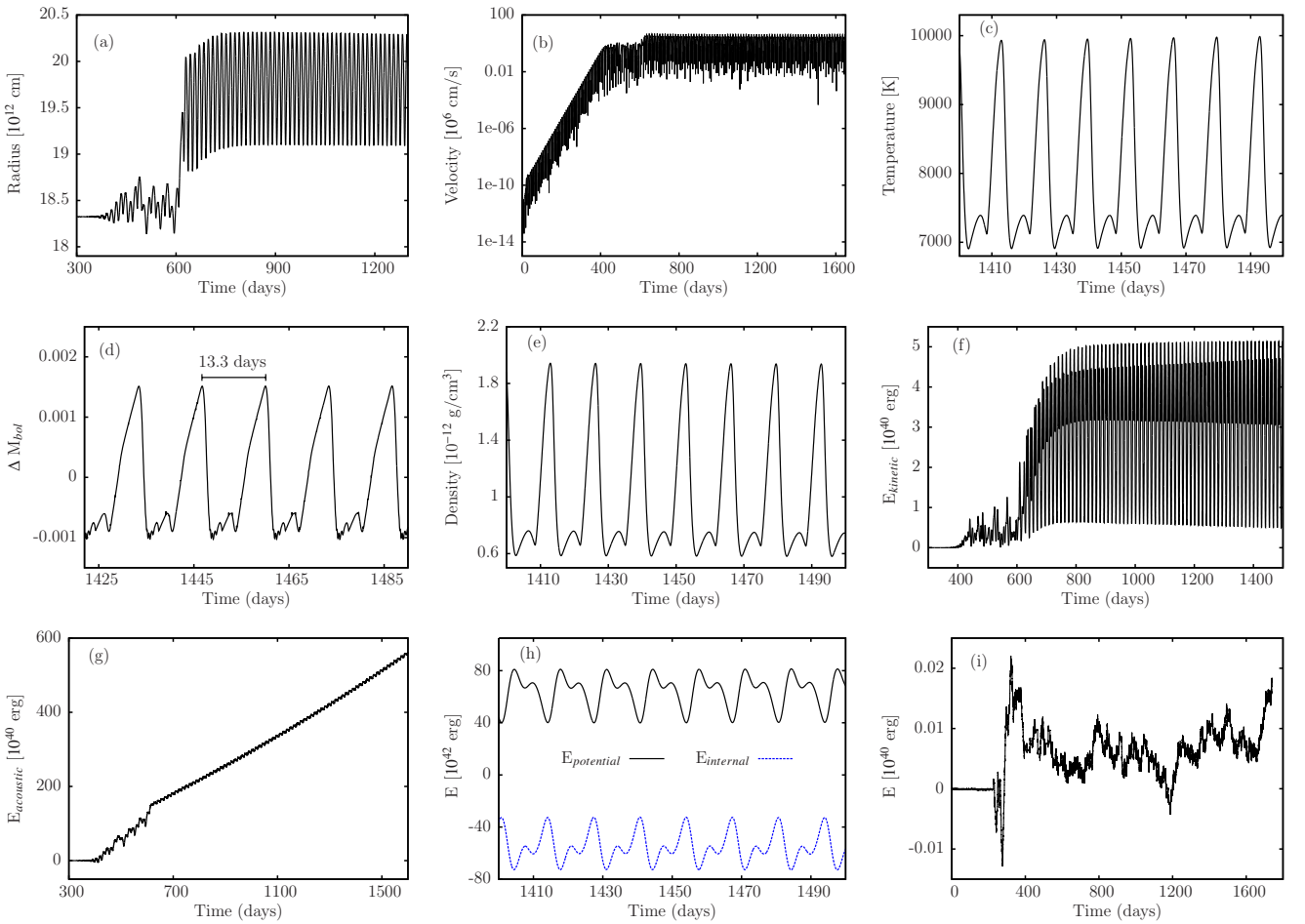


**Figure 10.** Evolution of instabilities into the non-linear regime for a model having  $M = 150 M_{\odot}$  and  $\log T_{\text{eff}} = 4.2$ . Radius (a), velocity (b), temperature (c) and density (e) at the outermost grid point, and the variation of the bolometric magnitude (d) are shown as a function of time. From the evolution of the velocity (b), we deduce that the evolution of the instability starts from hydrostatic equilibrium with velocity perturbations of the order of  $10^{-7} \text{ cm s}^{-1}$  superimposed, undergoes the linear phase of exponential growth and saturates in the non-linear regime with an amplitude of  $30 \text{ km s}^{-1}$ . Compared to the hydrostatic value, the mean radius is increased by  $\approx 8$  per cent in the non-linear regime. Some terms in the energy balance (with hydrostatic values subtracted) are given in (f)-(h) as a function of time. Potential and internal energy (h) with almost identical modulus have opposite sign. They are bigger than the kinetic (f) and the time integrated acoustic energy (g) by three and one orders of magnitude, respectively. The error in the energy balance is shown in (i). It is smaller than the smallest term in the energy balance by at least two orders of magnitude.

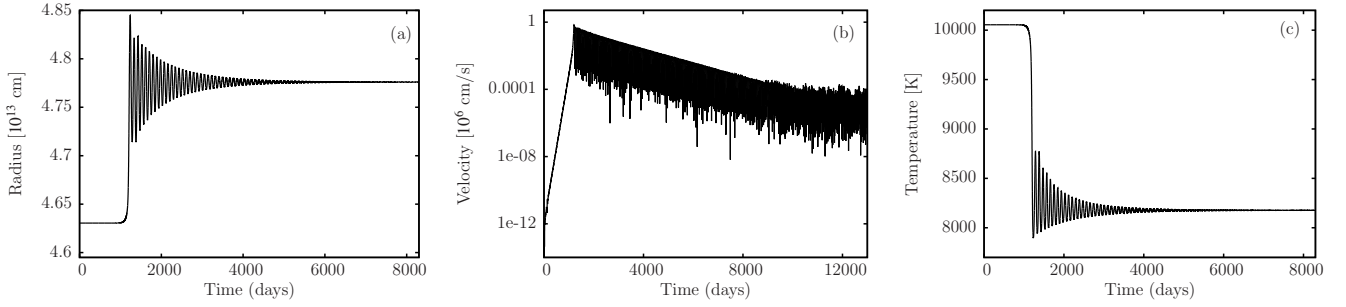


**Figure 11.** Same as Fig. 9 but for a model having  $M = 150 M_{\odot}$  and  $\log T_{\text{eff}} = 4.0$ . Note the presence of a monotonically unstable mode in the linear phase of exponential growth. The instability rearranges the stellar structure and a new hydrostatic state with slightly increased radius and decreased effective temperature is attained.

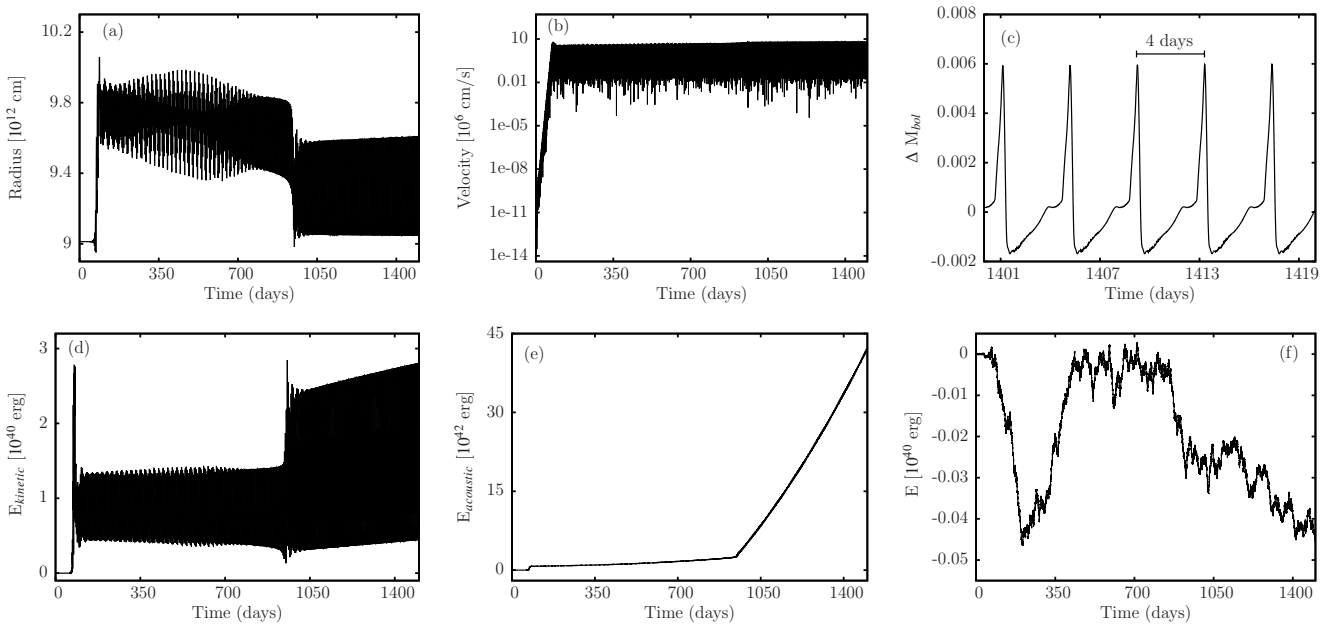


**Figure 12.** Evolution of instabilities and finite amplitude pulsations for a model having  $M = 200 M_{\odot}$  and  $\log T_{\text{eff}} = 4.4$ . As a function of time, the stellar radius, the velocity at the outermost grid point and the variation of the bolometric magnitude are displayed in (a)-(c), respectively. The velocity amplitude reaches  $53 \text{ km s}^{-1}$  in the non-linear regime. Kinetic energy, time integrated acoustic energy at the outer boundary and the error in the energy balance are shown in (d)-(f), respectively.

tional boundary conditions (see Fig. 2). Starting from numerical noise, the evolution of the instability (see Fig. 11) exhibits a linear phase of monotonic exponential growth (with the growth rate predicted by the linear analysis) saturating in the non-linear regime with a velocity amplitude below  $10 \text{ km s}^{-1}$ . In this phase, the structure becomes sufficiently modified to ensure stabilization and the configuration starts to oscillate around a new hydrostatic equilibrium with an exponential decay of the superimposed perturbations. The decay of the velocity perturbations ends on the numerical noise level.

From our study, we conclude that the model which is linearly unstable independent of the boundary conditions ( $\log T_{\text{eff}} = 4.2$ , Fig. 10) finally exhibits finite amplitude pulsations (including mass-loss), whereas instabilities caused by the boundary conditions only ( $\log T_{\text{eff}} = 4.6, 4.4, 4.0$ ; Figs. 8, 9, 11) lead to modified hydrostatic equilibria. Thus, with respect to the final fate of the model (hydrostatic equilib-

rium or finite amplitude pulsations with mass-loss) the dependence on boundary conditions of the linear stability analysis becomes less important (see the discussion in section 4).

## 5.2 Models with masses of $200 M_{\odot}$ and $250 M_{\odot}$

Similar to the unstable models with masses of  $150 M_{\odot}$  ( $\log L/L_{\odot} = 6.6$ ), we have performed non-linear simulations of the evolution of instabilities into the non-linear regime for unstable models with  $200 M_{\odot}$  and  $250 M_{\odot}$  ( $\log L/L_{\odot} = 6.77$  and  $6.88$ ). As examples, we present results for the models with  $\log T_{\text{eff}} = 4.4$  (which are unstable independent of boundary conditions) in Figs. 12 and 14. For both  $200$  and  $250 M_{\odot}$ , the instability leads to finite amplitude pulsations with a final period of  $4.0$  and  $4.8$  days and velocity amplitudes of  $53$  and  $56 \text{ km s}^{-1}$ , respectively. From the mean slope of the time integrated acoustic energy, we estimate a mass-loss rate of  $5.4 \times 10^{-6}$  and  $5.3 \times 10^{-6} M_{\odot} \text{ yr}^{-1}$ , respectively.



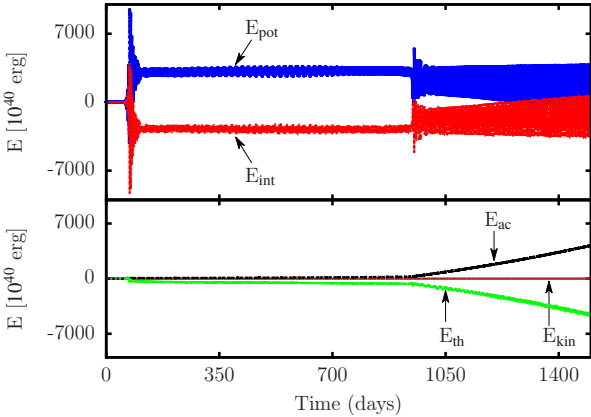


**Figure 13.** Potential, internal, kinetic, time integrated acoustic and time integrated thermal energy (at the outer boundary) as a function of time for a model with  $M = 200 M_{\odot}$  and  $\log T_{\text{eff}} = 4.4$ . Potential and internal energies with almost identical modulus and opposite sign are bigger than the kinetic energy by several orders of magnitude. Opposite signs and similar moduli of the mean slope of time integrated acoustic and thermal energies indicate that through the finite amplitude pulsations, thermal energy flux is transformed into acoustic energy flux.

We emphasize again the importance of conservativity with respect to energy (see Figs. 12, 14 d and f).

A comparison of the various terms occurring in the energy balance (see equation 23 of Grott et al. 2005) provide inside into the energy source for the pulsationally driven wind: Potential, internal, kinetic, time integrated acoustic and time integrated thermal energy (at the outer boundary) as a function of time are displayed in Fig. 13 for the model with  $M = 200 M_{\odot}$ . Potential and internal energies with almost identical modulus and opposite sign are bigger than the kinetic energy by several orders of magnitude. Opposite signs and similar moduli of the mean slope of time integrated acoustic and thermal energies indicate that through the finite amplitude pulsations, thermal energy flux is transformed into acoustic energy flux.

The results of our simulations are summarized in table 1, where final pulsation periods and mass-loss rates are given as a function of mass and effective temperature. Apart from a dependence on the strength of the underlying instability of the mass-loss rate, the latter seems to increase with mass and luminosity.

## 6 DISCUSSION AND CONCLUSIONS

A linear stability analysis has been performed for primordial post main sequence stellar models with masses between 150 and 250  $M_{\odot}$  (corresponding to luminosities between  $\log L/L_{\odot} = 6.6$  and 6.88) covering the range of effective temperatures between  $\log T_{\text{eff}} = 4.80$  and 3.62. The luminosity to mass ratios of these models lie between  $2.6 \times 10^4$  and  $3.0 \times 10^4$  (solar units) and suggest the existence of strange mode instabilities with growth rates in the dynamical range which typically occur for luminosity to mass ratios in excess of  $10^3$  (Gautschy & Glatzel 1990b; Glatzel 1994).

Contrary to previous investigations (Moriya & Langer 2015), the expected strange mode instabilities have in fact

been discovered, however only below an effective temperature of  $\log T_{\text{eff}} \approx 4.5$ . These findings are consistent with the predictions of a model for strange mode instabilities proposed by Glatzel (1994). According to it, in addition to high luminosity to mass ratios, a non-vanishing derivative of the opacity with respect to density is required for the existence of strange mode instabilities. For temperatures above  $\log T_{\text{eff}} \approx 4.5$ , the matter in the stellar envelope is completely ionized and for primordial chemical composition ( $Z = 0$ ) only electron scattering contributes to the opacity. Since the latter is constant, the derivative of opacity with respect to density vanishes and - according to the model and in agreement with our findings - no strange mode instabilities do occur. On the other hand, if the effective temperature falls below  $\log T_{\text{eff}} \approx 4.5$ , helium recombines and its bound-free transitions contribute to the opacity resulting in a finite derivative of opacity with respect to density. Thus according to the model, strange mode instabilities should appear together with helium recombination for temperatures below  $\log T_{\text{eff}} \approx 4.5$ , which agrees perfectly with our results. We may thus take our results as a confirmation of the strange mode model introduced by Glatzel (1994).

A second type of instabilities was identified for effective temperatures below  $\log T_{\text{eff}} \approx 3.7$ . The energy transport in the envelopes of models affected by this instability is almost entirely due to convection. As any linear stability analysis developed so far does not contain a satisfactory treatment of convection, we refrain from further speculations concerning possible implications and consequences of this instability. In particular, contrary to Moriya & Langer (2015) we have not performed simulations of the evolution of this instability into the non-linear regime.

For selected stellar models, the evolution of strange mode instabilities into the non-linear regime was followed by numerical simulations. Except for models, where the instability is caused by a special choice of boundary conditions (in these cases a modified hydrostatic equilibrium is the consequence of the instability) strange mode instabilities in primordial post main sequence models were found to lead to finite amplitude pulsations with velocity amplitudes of the order of  $50 \text{ km s}^{-1}$ . Associated with these pulsations are acoustic energy fluxes capable of driving winds with mass-loss rates up to  $3.5 \times 10^{-4} M_{\odot} \text{ yr}^{-1}$ . That these mass-loss rates are smaller than those derived by Moriya & Langer (2015) by at least two orders of magnitudes, is noteworthy. The post main sequence phase of the primordial stars studied lasts for  $10^4 - 10^5$  years. Even the maximum mass-loss rates determined here would then influence the evolution of these objects at most marginally.

We emphasize that extremely high accuracy requirements have to be satisfied for the numerical treatment of stellar instabilities and pulsations which can only be met by a with respect to energy fully conservative scheme. They are due to the fact, that the kinetic energies and the acoustic energy fluxes to be determined here, are smaller than the dominant gravitational and internal energies by several orders of magnitude. In the simulations performed by Moriya & Langer (2015) the kinetic energies reach a level ( $10^{47}$  ergs) which is typical for gravitational and internal energies but not for kinetic energies. We suspect that the numerical scheme adopted by these authors is not conservative and the kinetic energies live on the numerical error

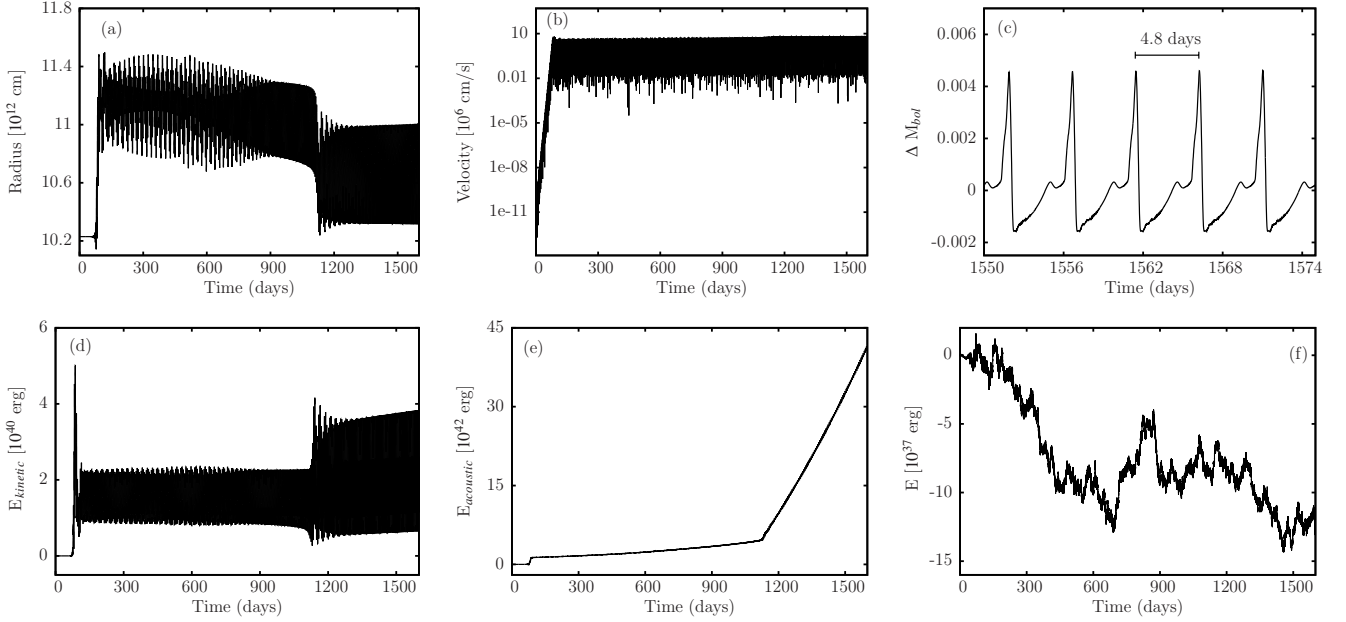


**Figure 14.** Evolution of instabilities and finite amplitude pulsations for a model having  $M = 250 M_{\odot}$  and  $\log T_{\text{eff}} = 4.4$ . As a function of time, the stellar radius, the velocity at the outermost grid point and the variation of the bolometric magnitude are displayed in (a)-(c), respectively. The velocity amplitude reaches  $56 \text{ km s}^{-1}$  in the non-linear regime. Kinetic energy, time integrated acoustic energy at the outer boundary and the error in the energy balance are shown in (d)-(f), respectively.

**Table 1.** Pulsation periods and mass-loss rates for the primordial stellar models selected.

Mass ( $M_{\odot}$ )	$\log T_{\text{eff}}$ (K)	Pulsation Period (days)	Mass Loss Rate ( $M_{\odot} \text{ yr}^{-1}$ )
150	4.6	Stable	—
	4.4	Stable	—
	4.2	13.3	$7.7 \times 10^{-7}$
	4.0	Stable	—
200	4.4	4.0	$5.4 \times 10^{-6}$
	4.2	20.0	$2.58 \times 10^{-6}$
250	4.4	4.8	$5.3 \times 10^{-6}$
	4.2	25.3	$3.5 \times 10^{-4}$

of the gravitational and internal energies. This would cast severe doubts on the reliability of this investigation, in particular on the high mass-loss rates claimed. We note that the numerical calculations presented by Appenzeller (1970) suffer from the same problem.

Strange modes and associated instabilities are not restricted to radial perturbations and have been identified for non-radial perturbations as well (see e.g., Glatzel & Mehren 1996; Glatzel & Kaltschmidt 2002). Therefore we suspect the presence of unstable strange modes in massive primordial stars for non-radial perturbations too. A linear stability analysis for non-radial perturbations will be presented in a forthcoming study.

## ACKNOWLEDGEMENTS

APY gratefully acknowledges financial support through a SmartLink Erasmus Mundus Post-Doc fellowship.

## REFERENCES

- Abel T., Bryan G. L., Norman M. L., 2000, *ApJ*, **540**, 39  
 Appenzeller I., 1970, *A&A*, **5**, 355  
 Baker N., Kippenhahn R., 1962, *Z. Astrophys.*, **54**, 114  
 Baker N., Kippenhahn R., 1965, *ApJ*, **142**, 868  
 Baraffe I., Heger A., Woosley S. E., 2001, *ApJ*, **550**, 890  
 Barkana R., Loeb A., 2001, *Phys. Rep.*, **349**, 125  
 Böhm-Vitense E., 1958, *Z. Astrophys.*, **46**, 108  
 Bromm V., Larson R. B., 2004, *ARA&A*, **42**, 79  
 Bromm V., Coppi P. S., Larson R. B., 1999, *ApJ*, **527**, L5  
 Bromm V., Coppi P. S., Larson R. B., 2002, *ApJ*, **564**, 23  
 Fosbury R. A. E., et al., 2003, *ApJ*, **596**, 797  
 Gautschi A., Glatzel W., 1990a, *MNRAS*, **245**, 154  
 Gautschi A., Glatzel W., 1990b, *MNRAS*, **245**, 597  
 Glatzel W., 1994, *MNRAS*, **271**, 66  
 Glatzel W., Kaltschmidt H. O., 2002, *MNRAS*, **337**, 743  
 Glatzel W., Mehren S., 1996, *MNRAS*, **282**, 1470  
 Grott M., Chernigovski S., Glatzel W., 2005, *MNRAS*, **360**, 1532  
 Iglesias C. A., Rogers F. J., 1996, *ApJ*, **464**, 943  
 Kashlinsky A., Arendt R. G., Mather J., Moseley S. H., 2005,

- [Nature](#), **438**, 45
- Kippenhahn R., Weigert A., Weiss A., 2012, *Stellar Structure and Evolution*, [doi:10.1007/978-3-642-30304-3](#).
- Loeb A., Barkana R., 2001, [ARA&A](#), **39**, 19
- Moriya T. J., Langer N., 2015, [A&A](#), **573**, A18
- Nomoto K., Kobayashi C., Tominaga N., 2013, [ARA&A](#), **51**, 457
- Ohkubo T., Nomoto K., Umeda H., Yoshida N., Tsuruta S., 2009, [ApJ](#), **706**, 1184
- Rogers F. J., Iglesias C. A., 1992, [ApJS](#), **79**, 507
- Rogers F. J., Swenson F. J., Iglesias C. A., 1996, [ApJ](#), **456**, 902
- Tumlinson J., Shull J. M., 2000, [ApJ](#), **528**, L65
- Yadav A. P., Glatzel W., 2016, [MNRAS](#), **457**, 4330
- Yadav A. P., Glatzel W., 2017a, [MNRAS](#), **465**, 234
- Yadav A. P., Glatzel W., 2017b, [MNRAS](#), **471**, 3245

This paper has been typeset from a  $\text{\TeX}/\text{\LaTeX}$  file prepared by the author.